Methods

Vector construction

Mammalian codon-optimized sequences of opto-α_1AR and opto-β_2AR (amino acid sequences in Fig. 1a) were synthesized and cloned into pcDNA3.1, and fused to the N-terminus of mCherry or YFP (with its start codon deleted) using the NotI site. The linker between the optoXR and mCherry/YFP is 5'-GCGGCCGCC-3'. Lentiviral vectors containing Synapsin I-optoXR-mCherry were constructed by cloning the transgene for each optoXR-mCherry into the AgeI and EcoRI sites of the pLenti-SynapsinI-hChR2-mCherry-WPRE vector described previously[1].

Lentiviral Production

High-titer lentivirus was produced as described[1]. Briefly, HEK 293FT cells were plated to 90% confluence in a 4-layer cell factory (Nunc) cultured with DMEM containing 10% FBS. Cells were co-transfected with 690 µg of the lentiviral vector described above and two helper plasmids (690 µg of pΔCMVR8.74 and 460 µg of pMD2.G). Media was changed at 15 h post-transfection. At 24 h post-transfection, media was changed with 200-220 mL of serum-free UltraCULTURE (Cambrex) containing 5 mM sodium butyrate. At 40 h post-transfection, the culture supernatant now containing virus was spun at 1000 rpm for 5 min to remove cellular debris and then filtered using a 0.45 µm low-protein-binding filter flask. The clarified supernatant was then ultra-centrifuged for 2 h at 55,000g using an SW-28 rotor (Beckman) to precipitate the virus. After centrifugation, supernatant was discarded and the resultant viral pellet was dissolved in a total of 100 µL of cold (4°C) PBS. The resuspended virus was centrifuged for 5 min at 7000 rpm to remove remaining cellular and viral debris. Aliquots were frozen at -80°C until further use.

Animal surgery and behavior

Female C57BL/6 mice, 10-12 weeks old, were housed and handled according to the Laboratory Vertebrate Animals protocol of Stanford University. Virus solution was delivered to the right nucleus accumbens as follows. Animals were anaesthetized under isoflurane and fur was sheared from the top of the head. While under isoflurane anesthesia, the head of the animal was placed in a stereotactic frame (David Kopf Instruments). A midline scalp incision was made and a ~1 mm diameter craniotomy was drilled 1.10mm anterior, and 1.45 mm lateral to bregma. A beveled 33-gauge needle (NanoFil, World Precision Instruments) pre-loaded with virus was then lowered into the accumbens (needle tip at 4.70-4.80 mm ventral to bregma) and 1.0 µL of virus was injected at 100 nL/min using an automated syringe pump (NanoFil, World Precision Instruments). Following injection, 3-5 min was allowed for tissue relaxation and fluid diffusion before retraction of the needle. For animals targeted for acute slice or in vivo recording experiments, the craniotomy was filled with dental cement (Lang Dental) and the incision was closed using VetBond (3M). For animals targeted for behavioral analysis, cannulas (C316G, cut 4.5 mm below the pedestal; PlasticsOne) were placed with the pedestal flush to the skull. Cannulae were secured using Metabond (Parkell) and dental cement (Lang Dental). Following drying of VetBond or cement, animals were removed from the frame and allowed to recover for at least one week before further manipulation. Control animals for behavioral experiments underwent the same manipulations

(surgery, cannula implantation, light stimulation) as experimental animals, and were injected with vehicle (PBS) alone instead of virus. For place preference experiments, animals that did not show a baseline preference for either side chamber (>70% or <10%) or for the central chamber (>40%) were admitted into the study; >90% of all animals met these criteria for an unbiased, balanced place preference design[2].

Acute slice preparation

Animals were anaesthetized under isoflurane and decapitated using surgical shears (Fine Science Tools). Coronal, 275 μm-thick slices containing accumbens were cut and stored in a cutting solution containing 64mM NaCl, 2.5mM KCl, 1.25mM NaH_2PO_4, 25mM $NaHCO_3$, 10mM glucose, 120mM sucrose, 0.5mM $CaCl_2$ and 7mM $MgCl_2$ (equilibrated with 95% O_2/5% CO_2). Following slicing, slices were incubated in the cutting solution at 32-35°C for 30 min and then at room temperature until experimentation. For *ex vivo* optoXR stimulation, slices were loaded on the stage of an upright microscope (BX51W, Olympus) and perfused with an artificial cerebrospinal fluid containing 124mM NaCl, 3mM KCl, 1.25mM NaH_2PO_4, 26mM $NaHCO_3$, 10mM glucose, 2.4mM $CaCl_2$, and 1.3mM $MgCl_2$ (equilibrated with 95% O_2/5% CO_2). Light from a 300W Lambda DG-4 (Sutter) was passed through a 473 nm ± 20 nm bandpass filter (Semrock) and applied to the slices using a 4X objective (0.28 NA) for 10 min followed immediately by fixation for later analysis.

Signaling validation assays

HEK293FT cells (Invitrogen) were transfected using Lipofectamine 2000 (Invitrogen) in 24-well plates and changed to serum-free medium 4-6hrs post-transfection. For Ca^{2+} imaging (Fig. 1c), cells plated on matrigel-coated coverslips were loaded with 5μg/ml fura-2 AM in F-127 Pluronic/DMSO (Probes) in Tyrode containing 1μM ATR, at 37°C and 5% atmospheric CO_2 for 20-25min. Following loading, coverslips were imaged at 340nm/380nm on an Olympus BX51W using Metafluor (Axon Instruments) controlling a 300W Lambda DG-4 (Sutter). For immunoassays (Fig. 2a, S1a), 18-24hrs after transfection, 1μM ATR and 50mM LiCl (to prevent IP_1 degradation) were added and plates transferred to an environmentall-controlled microscope (Leica DMI6000; 37°C, 5% atmospheric CO_2). 5 regions/well were optically stimulated for 1 min each (Sutter 300W Lambda DG-4; Semrock 504/12nm bandpass filter; 10X 0.30 NA objective); 3 wells/condition. Following incubation (cAMP/cGMP: 20min; IP_1: 1hr), cells were lysed and analyze by HTRF (CisBio) and a Biotek Synergy4 reader.

Immunohistochemistry and confocal analysis

Following *in vivo* stimulation, mice were transcardially perfused with ice-cold 4% paraformaldehyde (PFA) in PBS (pH 7.4) 90 min after termination of stimulation. Brains were removed and fixed overnight in 4% PFA and then equilibrated in 30% sucrose in PBS. Coronal, 40 μm-thick sections were cut on a freezing microtome and stored in cryoprotectant at 4°C until processed for immunohistochemistry. Free-floating sections were washed in PBS and then incubated for 30 min in 0.3% Tx100 and 3% normal donkey serum (NDS). For acute slice experiments, immediately following stimulation the 275 μm-thick slices were fixed for 1 hr in ice-cold 4% PFA and incubated with 0.5% Tx100 and 3% NDS. For MAPK assays (Fig. S1, top), immediately following HEK293 cell stimulation (completed as in Fig. 2a), coverslips were fixed for 15min, incubated with 0.6% H_2O_2 and then permeabilized with 0.1% Tx100 in 3% NDS.

Primary antibody incubations were conducted overnight in 0.01% Tx100 and 3% NDS for mouse anti-GAD67 1:500, Millipore, Billerica, MA; rabbit anti-cfos 1:500, Calbiochem, San Diego, CA; rabbit anti-phospho-CREB Ser133 1:500, Millipore. Sections were washed and incubated with secondary antibodies (1:1000) conjugated to either FITC or Cy5 (Jackson Laboratories, West Grove, PA) for 3 hrs at room temperature. Following 20 min incubation with DAPI (1:50,000) sections were washed and mounted on microscope slides with PVD-DABCO. The remaining overnight primary antibody incubations (rabbit anti-phosphoErk1/2; anti-phospho-MAPK p38 1:500, Promega, Madison, WI; mouse monoclonal anti-dopamine D1 receptor 1:50, Chemicon; rabbit polyclonal anti-dopamine D2 receptor 1:50, Millipore; goat polyclonal anti-choline acetyltransferase 1:200, Millipore) were followed by incubation with biotinylated secondary antibody (1:500, Jackson Laboratories), avidin-biotin-horseradish peroxidase treatment (ABC kit, Vector Labs, Burlingame, CA), and TSA detection (Perkin Elmer, Shelton, CT) according to manufacturer's instructions.

Confocal fluorescence images were acquired on a Leica TCS SP5 scanning laser microscope using a 20X/0.70NA or a 40X/1.25NA oil immersion objective. Four serial stack images per condition were acquired within a 500 µm region beneath the cannula tract. DAPI staining was used to delineate nuclei for determination of the mean pixel intensity of cfos or pCREB immunoreactivity using Volocity (Improvision) software. Positive or pCREB-active cells were identified by intensity threshold, and image acquisition and analysis were performed blind to the experimental conditions.
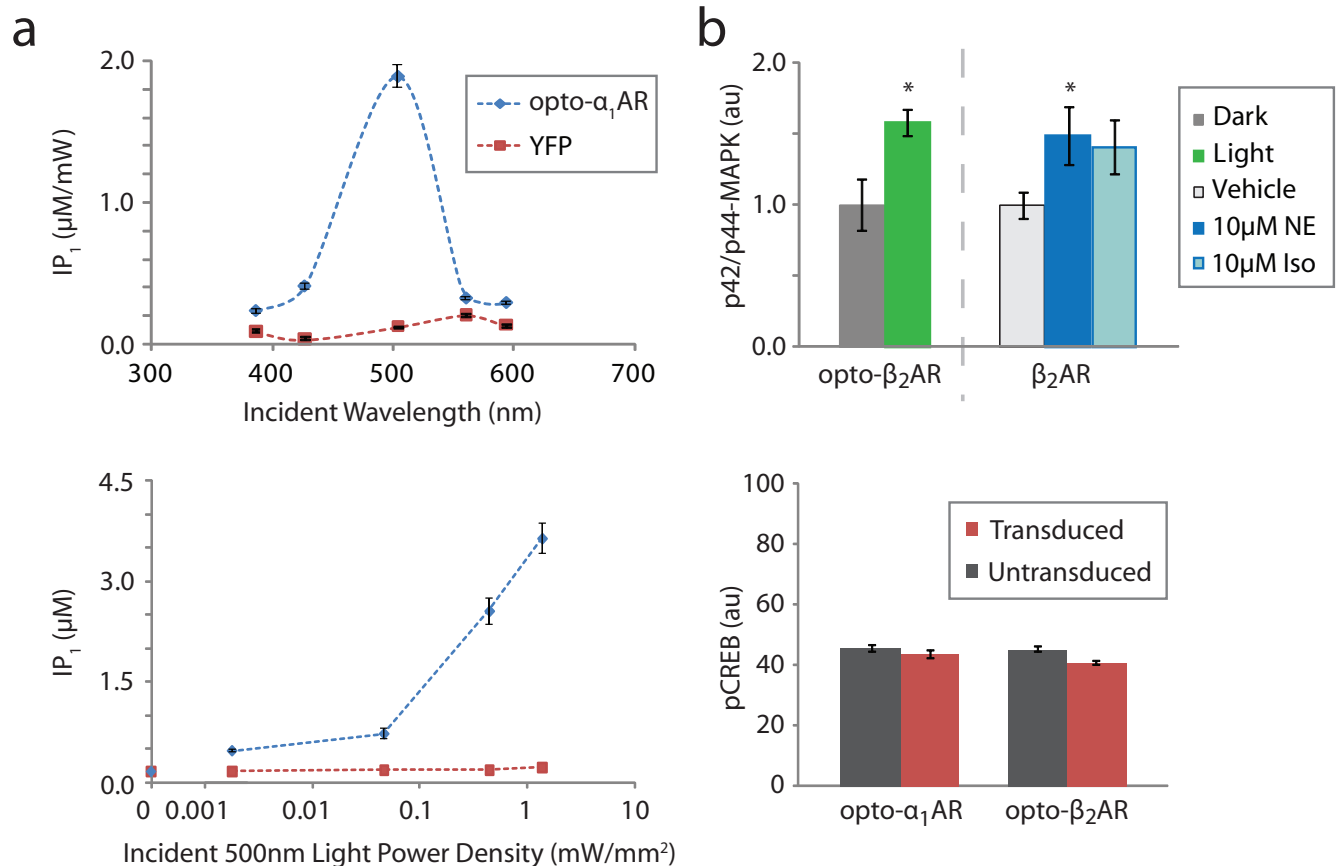
Figure S1: optoXR control of biochemical signaling

a) *Top*: Action spectra of indicated constructs. 1 min/field of optical stimulation was delivered through bandpass filters centered on indicated wavelengths through a 10X objective; IP_1 produced was measured following stimulation, and normalized by incident power of light. *Bottom*: Light responsivity of indicated constructs. IP_1 was quantified following 1 min/field of indicated power flux of 500nm light stimulation. b) *Top*: p42/p44-MAPK activation can be induced by stimulating opto-β_2AR with efficacy comparable to either 10 μM norepinephrine (NE) or 10 μM isoproterenol (Iso) acting on the wild-type β_2-adrenergic receptor (β_2AR). Data were normalized to the control mean of cells transfected with fluorescent protein (YFP) alone and to the baseline control for each experimental round (Student's t-test versus baseline; *: $p < 0.05$). *Bottom*: To test for possible basal activity *in vivo*, animals transduced with the indicated construct but not acutely optically stimulated were fixed and sliced; pCREB was quantified in the transduced and the contralateral, untransduced accumbens. No significant increases in pCREB levels were seen in dark *in vivo*, consistent with *in vitro* results.
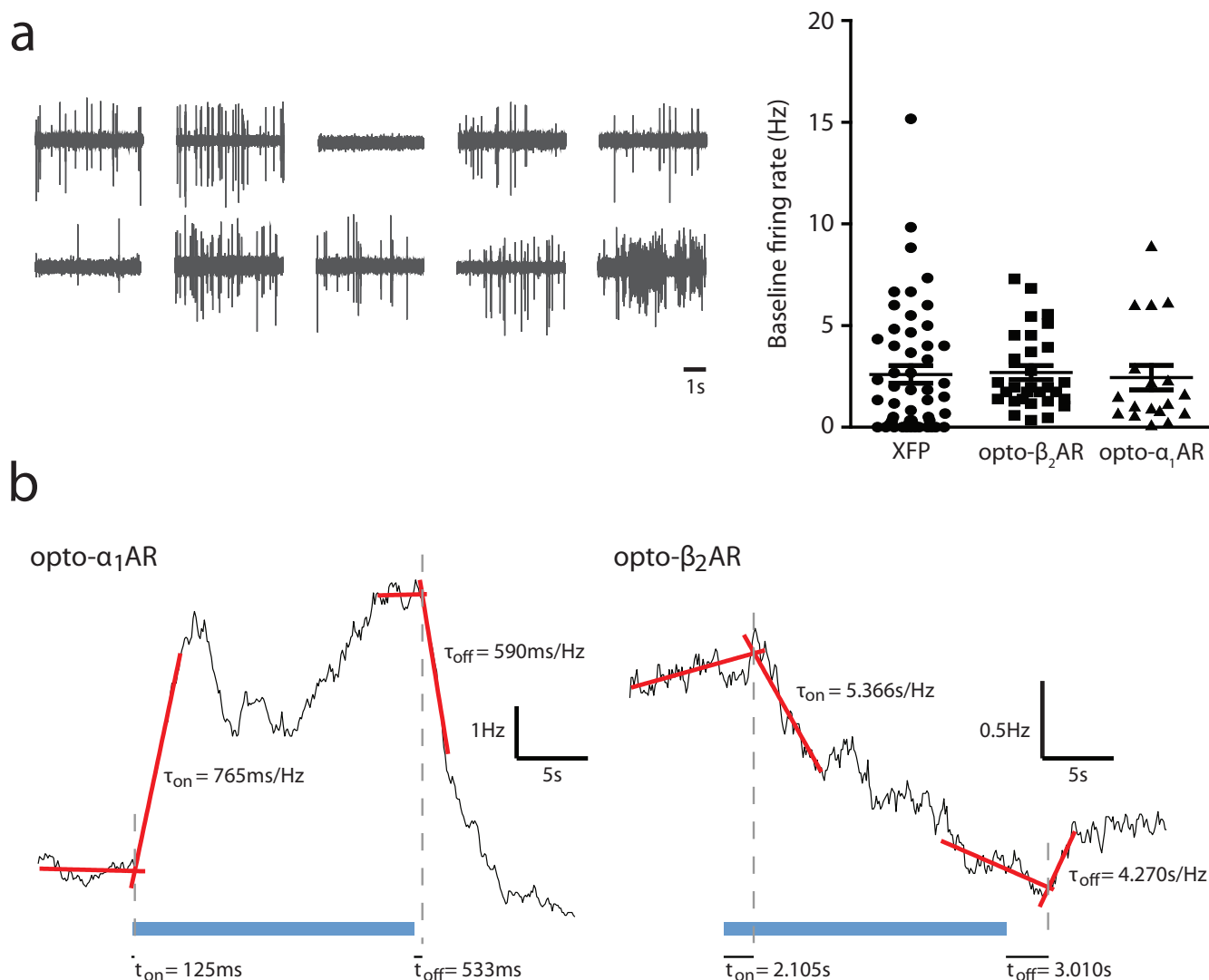
Figure S2: Kinetics of firing rate response to optoXR stimulation of accumbens

a) *Left*: Example traces of baseline firing in control accumbens transduced with fluorescent protein (mCherry) alone show typical variability in baseline firing rate from trace to trace. *Right*: Baseline firing rates of individual traces during recording of accumbens transduced with indicated construct. Mean +/- SEM firing rates shown in Figure 3a. b) Kinetics parameters describing firing rate changes after onset and offset of optical stimulation were obtained from linear fits to the spike firing histogram trendlines around light-on and light-off events (in red). The intersections of these lines were used to quantify the effective delay time to action (t) of optoXR stimulation. Rates of firing rate changes (τ) in turn were calculated as the reciprocal of the difference in the slopes of the lines surrounding each event. The effects on firing rate occurred faster and with larger magnitude with opto-α_1AR stimulation (t_{on}=125ms, t_{off}=533ms, τ_{on}=765ms/Hz, τ_{off}=590ms/Hz) than with opto-β_2AR stimulation (t_{on}=2.105s, t_{off}=3.010s, τ_{on}=5.366s/Hz, τ_{off}=4.270s/Hz). We observed no significant correlation between the baseline and the change in firing rates in either opto-α_1AR ($r^2 = 0.023$) traces or for the total population ($r^2 = 0.0205$). This correlation is only statistically significant for the opto-β_2AR subgroup ($r^2 = 0.347$), likely due to a floor effect given the relatively low basal rate of firing (~2.7Hz).
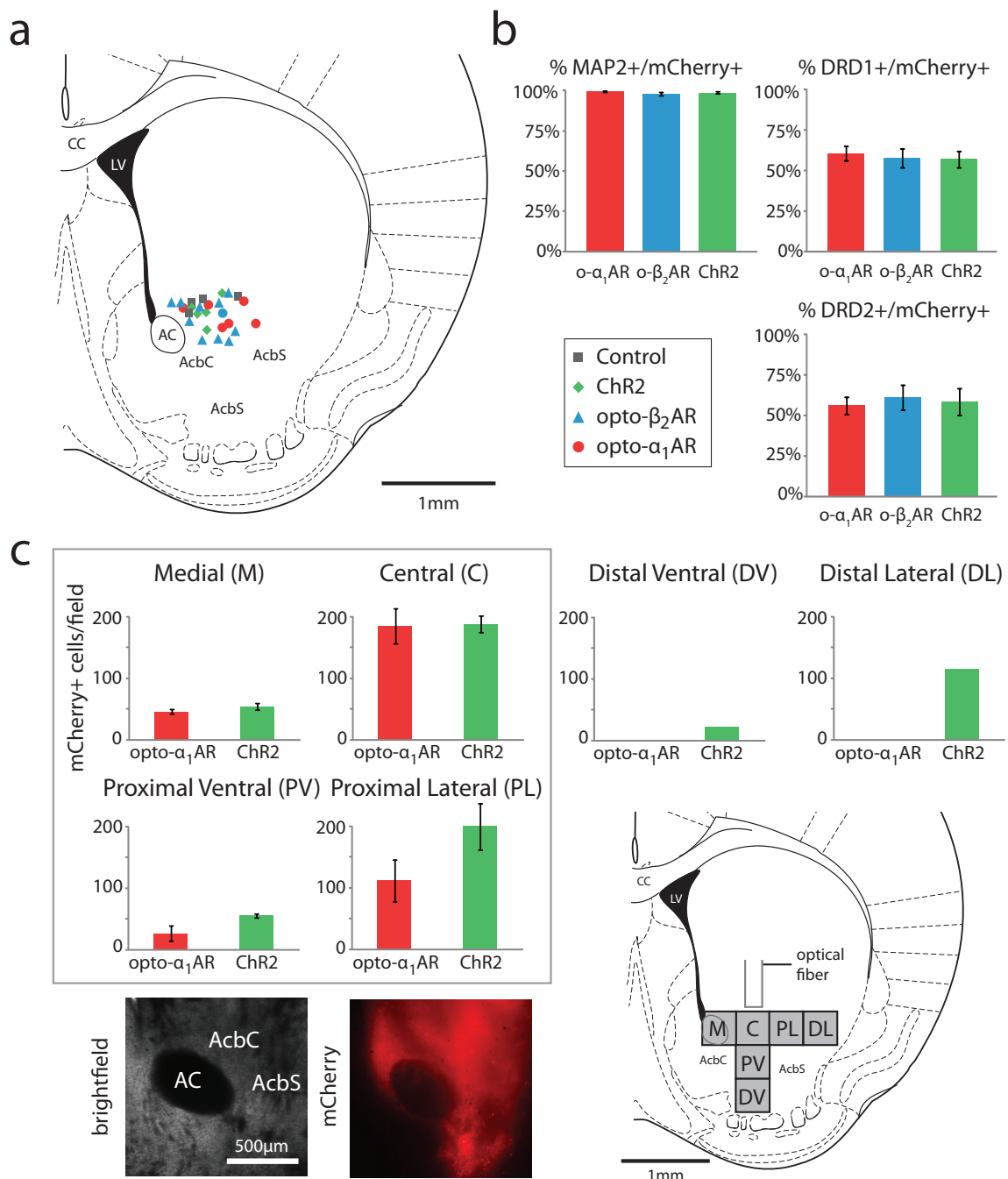
Figure S3: Summary of *in vivo* targeting and behavioral effects of optoXR stimulation

a) Cannula end placements for animals used in behavioral assays (Figs. 4, S4). Each symbol represents one animal. CC: corpus callosum; LV: lateral ventricle; AC: anterior commisure; AcbC: Core of nucleus accumbens; AcbS: Shell of nucleus accumbens. b) Percentage of mCherry+ cells that are also positive for marker indicated; no significant difference in cell phenotype between constructs for any marker tested. Extremely rare cells were also found stained for choline acetyltransferase (ChAT), with no significant difference in proportion of cells labeled. The temporal and cell-type precision of the optoXR method, restricting biochemical interventions to defined cells rather than a mixed population of afferent fibers, blood vessels, local neurons, glia, and fibers of passage, provides insight that could not have been achieved by other methods – it is important to note that these results do not restrict reward mechanisms to a single subclass of local neurons or to a specific pathway or neuromodulatory system, especially given the unknown role of ligand-biased signaling effects in these receptor pathways. c) Distribution of mCherry+ cells for animals presented in Fig. 4. Counts collected in corresponding field indicated on atlas in bottom right. No mCherry+ cells were observed medial to the "Medial" field, lateral to the "Distal Lateral" field, or ventral to the "Distal Ventral" field. *Bottom left*: Example brightfield (left) and mCherry (right) images of transduced accumbens.
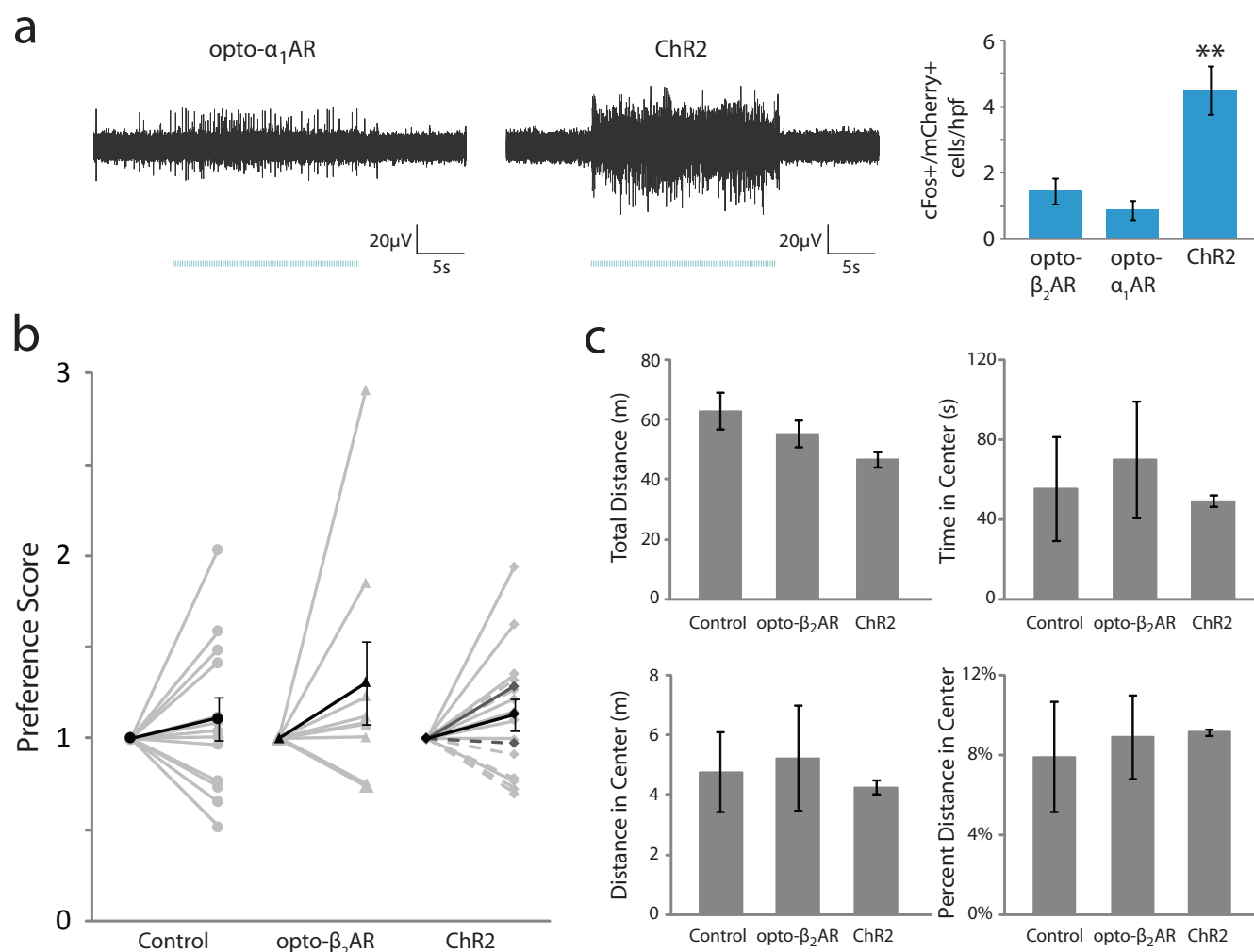
Figure S4: Behavioral results of opto-β_2AR and ChR2 stimulation *in vivo*

a) Left: Individual traces showing network response to 10Hz optical stimulation of indicated construct. Right: c-fos staining showing increased neuronal activation with ChR2 following 10Hz stimulation *in vivo* compared to optoXRs. (Student's t-test versus other constructs; **: $p < 0.01$) b) Individual (grey) and mean (black) scores for preference (fold increased time in conditioned chamber) for animals transduced with opto-β_2AR (n=9 animals) or ChR2 (n=15 animals) versus control as in Fig. 4; no significant differences were seen versus control (Student's t-test; $p > 0.05$). The circuit mechanisms determining efficacy of the modulated state in driving behavior could include promoting the throughput of distributed endogenous activity patterns with important spike timing relationships, or via promotion of neural circuit plasticity. Subsets of ChR2 animals were stimulated at either 3.8 Hz (dashed lines; n=7 animals) or 10 Hz (solid lines; n=8 animals); dark grey bars indicate means for each ChR2 subgroup (neither subgroup showed significant preference change); numerical scores in Table S4. c) Open field test (OFT) results; 10 Hz optical stimulation for each construct (as in Fig. 4). No significant differences were seen. Notably, previous studies have identified necessary roles in reward for G_q-linked systems including α_1AR[3,4], type I metabotropic glutamate receptors (mGluRs)[5-10], and PKC[11,12]; these data and Fig. 4 may complement those necessity studies by demonstrating that direct induction of a G_q-linked pathway is sufficient to drive behavioral reward. Possibly relevant G_q-linked receptor pathways could involve adrenergic input from the NTS[13,14], type I mGluRs[5,15-17], type 2 serotonin receptors[18], and G_q-coupled D1/D2 heterooligomers[19]; indeed, these results are not inconsistent with the importance of DA signaling in reward[20,21], particularly since DA and NE pathways interact[22,23].

Table S1

Raw numerical pCREB intensities (au) for data represented in Fig. 2b. Mean and SEM in bold for each subgroup; p-values for two-tailed t-test of subgroup versus control in italics.

	opto-α1AR		opto-β2AR	
mCherry	-	+	-	+
Mean	65.326	97.95309	63.6385	82.83284
SEM	3.758281	7.199024	3.847409	6.907057
p-value vs. mCherry-		*0.000272*		*0.019559*

Table S2

Raw numerical baseline firing rates (Hz) for data presented in Figs. 3a and S2a. Mean and SEM in bold for each subgroup; p-values for t-test of subgroup versus control in italics.

	XFP	oa1AR	ob2AR
Mean	2.596154	2.439357	2.687798
SEM	0.436406	0.603845	0.346556
p-value vs XFP		*0.834496*	*0.869791*

Table S3

Raw numerical changes in firing rate (Hz) for data presented in Fig. 3c calculated within the baseline itself ('Base') and between the baseline and the light stimulation periods ('Light').

	opto-β2AR		opto-α1AR	
	Base	Light	Base	Light
Mean	0.061788	-0.68113	-0.01287	3.816198
SEM	0.134665	0.162402	0.336387	0.812251
p-value vs Base		*0.000861*		*0.000239*

Table S4

Raw numerical preference scores (Ratio of Day 3/Day 1 times in conditioned chamber) for each animal represented in Figs. 4 and S4. Mean and SEM in bold for each subgroup; p-values for two-tailed t-test of subgroup versus control in italics.

	Control	ChR2 10Hz	ChR2 3.8Hz	opto-β2AR	opto-α1AR
Mean	1.1098	1.2686	0.9771	1.3076	1.5763
SEM	0.1184	0.1312	0.0984	0.2282	0.0927
p-value vs. Control	*0.3816*	*0.4003*	*0.4561*	*0.0053*	

total ChR2		
	Mean	1.1326
	SEM	0.0896
p-value vs. Control		*0.8795*

References

[1] Zhang, F., Wang, L.-P., Brauner, M. et al., *Nature* **446** (7136), 633 (2007).

[2] Olson, V. G., Heusner, C. L., Bland, R. J. et al., *Science* **311** (5763), 1017 (2006).

[3] Zhang, X. Y. and Kosten, T. A., *Biological Psychiatry* **57** (10), 1202 (2005).

[4] Drouin, C., Darracq, L., Trovero, F. et al., *Journal of Neuroscience* **22** (7), 2873 (2002).

[5] Popik, P. and Wróbel, M., *Neuropharmacology* **43** (8), 1210 (2002).

[6] Herzig, V. and Schmidt, W. J., *Neuropharmacology* **47** (7), 973 (2004).

[7] Herzig, V., Capuani, E., Kovar, K.-A. et al., *Addiction Biology* **10** (3), 243 (2005).

[8] Backstrom, P. and Hyytia, P., *Neuropsychopharmacology* **31** (4), 778 (2005).

[9] Lominac, K. D., Kapasova, Z., Hannun, R. A. et al., *Drug and Alcohol Dependence* **85** (2), 142 (2006).

[10] Chiamulera, C., Epping-Jordan, M. P., Zocchi, A. et al., *Nat Neurosci* **4** (9), 873 (2001).

[11] Aujla, H. and Beninger, R. J., *Behavioural Brain Research* **147** (1-2), 41 (2003).

[12] Narita, M., Akai, H., Nagumo, Y. et al., *Neuroscience* **127** (4), 941 (2004).

[13] Berridge, C. W., Stratford, T. L., Foote, S. L. et al., *Synapse* **27** (3), 230 (1997).

[14] Delfs, J. M., Zhu, Y., Druhan, J. P. et al., *Brain Research* **806** (2), 127 (1998).

[15] Coutinho, V. and Knopfel, T., *Neuroscientist* **8** (6), 551 (2002).

[16] McGeehan, A. J. and Olive, M. F., *Synapse* **47** (3), 240 (2003).

[17] Grueter, B., McElligott, Z., and Winder, D., *Molecular Neurobiology* **36** (3), 232 (2007).

[18] Cools, R., Roberts, A. C., and Robbins, T. W., *Trends in Cognitive Sciences* **12** (1), 31 (2008).

[19] Rashid, A. J., So, C. H., Kong, M. M. C. et al., *PNAS* **104** (2), 654 (2007).

[20] Tobler, P. N., Fiorillo, C. D., and Schultz, W., *Science* **307** (5715), 1642 (2005).

[21] Schultz, W., *Ann Rev Neuro* **30** (1), 259 (2007).

[22] Hyman, S. E., Malenka, R. C., and Nestler, E. J., *Ann Rev Neuro* **29** (1), 565 (2006).

[23] Weinshenker, D. and Schroeder, J. P., *Neuropsychopharmacology* **32** (7), 1433 (2006).